Journal Pre-proof

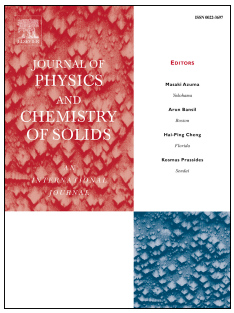

Structure rearrangements induced by lithium insertion in metal alloying oxide mixed spinel structure studied by x-ray absorption near-edge spectroscopy

S.J. Rezvani, Y. Mijiti, R. Gunnella, F. Nobili, A. Trapananti, M. Minicucci, M. Ciambezi, D. Bresser, S. Nannarone, S. Passerini, A. Di Cicco

PII: S0022-3697(19)31086-8

DOI: https://doi.org/10.1016/j.jpcs.2019.109172

Reference: PCS 109172

To appear in: *Journal of Physics and Chemistry of Solids*

Received Date: 13 May 2019

Revised Date: 24 July 2019

Accepted Date: 29 August 2019

Please cite this article as: S.J. Rezvani, Y. Mijiti, R. Gunnella, F. Nobili, A. Trapananti, M. Minicucci, M. Ciambezi, D. Bresser, S. Nannarone, S. Passerini, A. Di Cicco, Structure rearrangements induced by lithium insertion in metal alloying oxide mixed spinel structure studied by x-ray absorption near-edge spectroscopy, *Journal of Physics and Chemistry of Solids* (2019), doi: https://doi.org/10.1016/j.jpcs.2019.109172.

Structure rearrangements induced by lithium insertion in metal alloying oxide mixed spinel structure studied by x-ray absorption near-edge spectroscopy

S.J. Rezvani,[1,2] Y. Mijiti,[3] R. Gunnella,[3] F. Nobili,[4] A. Trapananti,[3] M. Minicucci,[3] M. Ciambezi,[3] D. Bresser,[5,6] S. Nannarone,[2] S. Passerini,[5,6] and A. Di Cicco[3]

[1] *Laboratori Nazionali di Frascati dell'Istituto Nazionale di Fisica Nucleare, Via Enrico Fermi, Frascati, Rome, Italy*
[2] *Consiglio Nazionale delle Ricerche (CNR), CNR-IOM, Bazovizza, Italy.*
[3] *Physics Division, School of Science and Technology, Università di Camerino, 62032 Camerino (MC), Italy*
[4] *Chemistry Division, School of Science and Technology, Università di Camerino, 62032 Camerino (MC), Italy*
[5] *Helmholtz Institute Ulm (HIU), Helmholtzstrasse 11, D-89081 Ulm, Germany*
[6] *Karlsruhe Institute of Technology (KIT), P.O. Box 3640, D-76021 Karlsruhe, Germany*

Carbon-coated $ZnFe_2O_4$ (ZFO-C) spinel ferrite nanoparticles can be used in electrodes for Li-ion batteries and are known to show capacities larger than those calculated for an ideal spinel structure. In this work, the local structure evolution and reordering of this material upon lithium insertion are studied using K-edge and L-edge x-ray absorption near edge spectroscopy (XANES). XANES simulations corresponding to different lithiation stages are performed using full multiple scattering (Fe, Zn K-edge, Zn L-edge) and ligand field multiplet (LFM) calculations (Fe L-edge). XANES simulations are compared with experimental spectra obtained on ZFO-C nanoparticles previously characterized by electrochemical measurements. It is shown that a satisfactory agreement for the XANES Fe and Zn K-edges of pristine ZFO-C bulk nanoparticles can be obtained introducing a mixed spinel structure with Fe and Zn partially occupying tetrahedral and octahedral sites. Upon lithiation, changes in the XANES spectra are interpreted introducing displacements of the cations as an effect of occupation of Li into empty lattice sites. In particular, comparison of the simulations with the XANES data indicates that reversible Li insertion is accompanied by a migration of the Zn and Fe atoms from tetrahedral to octahedral sites. Furthermore, by studying L-edge XANES spectra, we show that the relocation and valence change of metal ions occur at earlier lithiation stages at the surface of the active material, gradually extending to the bulk for larger Li uptakes.

I. INTRODUCTION

Metal conversion-alloying oxides have shown the capability of accommodating large number of alkali metal ions into their structure and hence are promising materials to be employed as battery electrodes[1,2]. Out of metal conversion-alloying oxides the ones with the spinel structure in particular have been serving as battery electrodes due to their high capacity of lithium uptake, being the lithium transport faster in closed pack arrays of the large polarizable anions[3–6]. Ideal Spinel structures have the general form $A[B_2]O_4$, where A refers to the cations on tetrahedral ($8a$) sites and B to the cations on octahedral ($16d$) sites of a cubic structure of the space group symmetry $Fd3m$. The oxygen anions are located at the $32e$ sites forming a cubic close packed array. A total of 64 tetrahedral sites are found, of which one-eighth are occupied by the A cations. On the other hand, one-half of the 32 octahedral sites are occupied by the B cations. Thus, it can be assumed that the unit cell of this spinel structure, with 56 empty tetrahedral sites and 16 empty octahedral sites, could easily accommodate the Li ions in the form of $[Li_x]_{16c}[A]_{8a}[B_2]_{16d}O_4$. Each empty tetrahedron and octahedron in the unit cell share at least two faces with the tetrahedral (A atoms) or octahedral sites (B atoms). Therefore, the short distances and coulombic interactions between a guest ion in an interstitial site and the A, B ions sitting in a neighboring site prevent the simultaneous occupation of the two. Lithium insertion is thus accompanied by an internal phase change (forcing the A atoms to move from $8a$ to $16c$ sites) that transforms the spinel arrangement to a new rock-salt cation structure in form of $[Li_xA]_{16c}[B_2]_{16d}O_4$[7–9].

Spinel ferrite $ZnFe_2O_4$ is one of the well known spinel structures that has shown a promising performance compared to the graphite electrodes. It has 2.7 times the capacity of the graphite with a relatively stable cycling performance. The lithiation mechanism in this structure is suggested to occur via insertion of Li ions into the vacant $16c$ sites for which at lower concentrations of the Li ions ($x < 1$) uptake occurs without structural evolution. However, at higher concentrations of the Li ions ($x > 1$) a displacement of the Zn atom to $16c$ sites due to the strong repulsive interaction is also expected[8,9]. It has also been suggested that this mechanism is accompanied by the reduction of the Fe ions which consequently leads to formation of amorphous metallic iron[10,11].

On the other hand, several works have shown that when normal spinel ferrite $ZnFe_2O_4$ becomes nano-sized, it can display a non-equilibrium cation distribution among tetrahedral and octahedral sites[12–14]. An expression for the mixed spinel structure of $ZnFe_2O_4$ can be written as $[Zn^{2+}_{1-y}Fe^{3+}_y]_{tet}[Zn^{2+}_yFe^{3+}_{2-y}]_{oct}O_4$ where y is an inversion coefficient corresponding to the degree of cation disorder. Iron (III) occupancy of both octahedral and tetrahedral sites in nanocrystalline $ZnFe_2O_4$ has been extensively proved by Mossbauer spectroscopy[15,16], nuclear magnetic resonance[17], neutron diffraction[18], x-ray absorption[13] and indirectly throughout magnetic measurements[19]. The inversion of Zn has been studied to a much lesser extent, although Extended X-ray Absorption Fine Structure (EXAFS) studies at Zn K-edge suggest that Zn ions move from their equilibrium positions to octahedral sites when the particle size decreases[20,21].

In particular, the lithium insertion mechanism in these nano particles can also be affected by the level of inversion and possibly improve the capacity of this material. Hence, a study aimed to clarify the structural evolution of spinel ferrite upon Li insertion in the presence of the cation disorders is well motivated.

In this work, we study the structural evolution and reordering of Li-ion electrodes made by carbon-coated $ZnFe_2O_4$ spinel ferrite nanoparticles (ZFO-C) upon lithium insertion, using the x-ray absorption spectroscopy (XAS, see for example[22,23] and refs. therein). This technique is particularly suited to study the details of the local structure around selected atomic species, so the environment of the Zn and Fe ions can be studied for different levels of lithiation. Accurate x-ray absorption near edge structures (XANES) experimental data at Fe and Zn K and L edge are compared with simulations in order to investigate the local structure around Zn and Fe ions and the degree of structural modifications induced by lithiation.

II. EXPERIMENT

A. Electrode preparation and electrochemical characterization

Carbon-coated ZnFe2O4 nanoparticles (ZFO-C) were synthesized by dissolving 0.75 g sucrose (Sigma-Aldrich) in 3.5 ml deionized water (Millipore) and subsequently adding 1.0 g nanoparticulate ZnFe2O4 (< 100 nm, > 99% trace metal basis, Sigma-Aldrich) under continuous stirring. The resulting mixture was homogenized by means of a planetary ball mill (Vario-Planetary Mill Pulverisette 4, FRITSCH; 800 rpm for 1.5 h) and afterwards dried overnight at 80 °C. The composite obtained was heated up to 500 °C for 4 h in a tubular furnace under Ar atmosphere with a heating ramp of 3°C min^{-1}. Eventually, the remaining powder was ground manually in an agate mortar for conducting all further experiments. The carbon coating layer thickness is between 2-5 nm.

ZFO-C electrodes were prepared by using sodium carboxymethylcellulose (Na-CMC, SigmaAldrich) dissolved in deionized water (5:95 w/w). ZFO-C and Super-P carbon (MMM-Carbon), previously mixed and ground in an agate

mortar, were added to the binder solution, and the resulting slurry was stirred for 5 h with a magnetic stirrer. The mixture was stratified on Cu foil (whose thickness is 10 μm; the surface was first wetted with acetone and scraped off with sandpaper) through the Doctor Blade technique and the thickness was set to 100 μm. The obtained layer was dried at room temperature for 30 min and in an oven at 55 °C overnight. The layer was then pressed by a roll press to a uniform thickness, resulting in an active mass loading of the order of about 1 mgcm^{-2}. Circular electrodes with a diameter of 9 mm and a surface area of 0.636 cm^2 were cut and dried overnight at 120 °C under vacuum. The capacity of electrodes has been calculated considering a specific theoretical capacity of 1000 mAhg^{-1}. Electrochemical measurements have been carried out by using three electrode T cells (Swagelock type), using electrodes as working electrode, and metallic lithium as counter and reference electrodes. A glass fibre (Whatman GF/A) has been used as separator, and a solution of $LiPF_6$ (0.5 M) in EC:DMC 1:1 v/v has been used as electrolyte. All of the cells have been assembled in a dry-box filled with Ar.

Samples for ex-situ XAS analysis have been prepared by submitting ZFO-C electrodes to selected Li uptakes via via galvanostatic discharge. Specific Li charging levels were chosen based on the expected effects of the lithium uptake in the structure of the active material and correspond to capacity and potential values of the electrodes that underwent XAS characterizations. First Point obtained at E=1.3 V and Q=49 mAhg^{-1} is related to the beginning of Li uptake by ZFO-C. Second and third points are obtained respectively at E=1.02 V, Q=83 mAhg^{-1} and at E=0.83 V, Q=167 mAhg^{-1}, correspond to the beginning and ending of a short voltage plateau with a high lithium uptake. Finally the fourth point was obtained at E=0.5 V and Q=836 mAhg^{-1} corresponding to the end of the main plateau.

B. X-ray absorption spectroscopy measurements

High-quality X-ray absorption spectroscopy (XAS) experiments on the electrodes were performed with special care during the preparation of samples. After suitable electrochemical characterizations as described in section II A, the cells have been disconnected. They were then disassembled and washed with dimethyl carbonate (DMC) to remove the electrolytic residuals. For Hard X-ray experiments, under Ar atmosphere, electrodes were dried and powder scrapped from the Cu current collector was mixed with ultra-pure cellulose and pressed into pellets. Samples were sealed in plastic bags suitable for X-ray experiments to preserve them from air and moisture exposure. For Soft X-ray experiments, electrodes were dried in an Ar atmosphere and kept in sealed packs while transported to the measurement chambers. Then the samples were placed in the XAS chambers via an argon controlled load lock chamber.

K-edge measurements: Fe and Zn K-edge XAS spectra of different electrodes at selected stages of lithium insertion (as described in section II A) were measured in scanning energy mode using a sagittally focusing double Si(311) crystal monochromator at the BM08 beam line[24] of the European Synchrotron Radiation Facility (ESRF). Two Pd coated mirrors working at an incidence angle of 3.6 mrad were used for harmonics rejection. The beam size at the sample was about 2×0.3 mm FWHM. XAS spectra were collected in fluorescence mode using a 12-elements high-purity Ge solid state detector and normalized by measuring the incident beam intensity with an ion chamber filled with Ar gas. The samples were installed in the standard BM08 experimental chamber, on a manipulator rotated by 45° with respect to the X-ray beam direction. XAS spectra in fluorescence mode were obtained by selecting a suitable photon energy window in the solid-state detector, enclosing the K_α Fe/Zn emission line related to the relaxation of the photo-excited atoms in the sample. XAS spectra of pure Fe and Zn placed in a second experimental chamber were acquired simultaneously with each sample scan for continuous monitoring of the energy scale against possible monochromator instabilities.

L-edge measurements Soft x-ray (Fe and Zn L-edge XAS) experiments were carried out using radiation at the exit of the 8.1 bending magnet of the ELETTRA synchrotron facility in Trieste (Italy) (BEAR end-station BL8.1L)[25]. The spectral energy was calibrated by referring to C $1\pi - 1\pi^*$ transitions. The incident light was horizontally polarized and the incidence angle of the light with respect to the sample surface plane was kept fixed at 10° with the s polarization. XAS measurements were done in total electron yield (TEY) mode and normalized to the incident photon flux. The TEY technique is surface sensitive, due to the limited probing depth (usually 2 - 10 nm[23]) related to the electron mean free path. An estimate of the probing depth related to TEY experiments at the Fe and Zn L-edge can be found in ref.[23] and result to be slightly different for the two edges: $\sim$ 6 nm (Fe L-edge, around 710 eV photon energy) and $\sim$ 9 nm (Zn L-edge, around 1020 eV photon energy).

III. COMPUTATIONAL PROCEDURE

K-edge simulations. Calculations of the XAS K-edge cross-section were performed within the multiple scattering theory, using MXAN[26] to run the CONTINUUM code for the calculation of the inverse scattering path operator[27]. The optical potential for phase-shift calculations included the real part of the Hedin-Lundqvist exchange potential and

the resulting cross-section was broadened using a convolution with a Lorentian function (Half-width HWHM $\Gamma = 0.35$ eV), for comparison with experimental data. Two kinds of spinel-type structure were adopted for the theoretical calculation, one being the ideal normal spinel $ZnFe_2O_4$ structure with space group $Fd3m$ and the other with an inverse spinel structure having Zn^{2+} ions residing on the octahedral site at $(\frac{1}{2}\frac{1}{2}\frac{1}{2})$, and Fe^{3+} ions on the tetrahedral sites at $(\frac{1}{8}\frac{1}{8}\frac{1}{8})$. Multiple-scattering calculations were performed for spherical-like clusters with a maximum cluster size $r = 8.44$ Å, verifying the convergence of the cross-section for increasing numbers of atoms. Calculations were also carried out for different stages of lithium insertion (see Table II) by inserting selected amounts of Li atoms at the expected crystallographic positions, following the structure evolution suggested by electrochemical measurements[10]. Furthermore, distinct atomic arrangements either via the inverse spinel or upon lithium uptake are considered in each case as reported in Tab. I and II).

Spinel	Structure	Position	No. atoms	No. Li	Cluster Size (Å)
Normal	$ZnFe_2O_4$	8a	251	0	8.44
	$ZnFe_2O_4$	16c	221	0	8.53
	$Li_{0.4}$ $ZnFe_2O_4$	8a	265	14	8.44
	$Li_{0.7}$ $ZnFe_2O_4$	8a	275	24	8.44
	$Li_{0.7}$ $ZnFe_2O_4$	16c	238	24	7.89
	$LiZnFe_2O_4$	16c	251	37	7.89
Inverse	$ZnFe_2O_4$	16d	227	0	8.44
Inverse	$Li_{0.4}ZnFe_2O_4$	16d	241	14	8.44
Inverse	$LiZnFe_2O_4$	16d	251	34	8.44

TABLE I. Parameters of Zn K-edge multiple scattering calculations via lithium insertion for both normal and inverted structure and considering the migration of Zn atoms.

Zn K-edge XAS calculations for normal and inverted spinel structures were carried out similarly as for Fe K-edge case, while calculations including migrated Zn atoms (to 16c sites) were performed using a cluster with dimension $r = 8.53$ Å as results from the new structural arrangement, in agreement with previous calculations reported in refs.[13,28]. The list of different calculations is reported in Tab. I. For example, in case of inversion/migration, a Zn atom is relocated at the octahedral 16c/16d site at the center of the spherical cluster and this position is used for the photo-absorber site in calculations.

Spinel	Structure	Position	No. atoms	No. Li	Cluster Size (Å)
Normal	$ZnFe_2O_4$	16d	227	0	8.44
	$Li_{0.4}$ $ZnFe_2O_4$	16d	241	14	8.44
	$Li_{0.7}$ $ZnFe_2O_4$	16d	253	26	8.44
	$LiZnFe_2O_4$	16d	261	34	8.44
	$Li_{1.5}$ $ZnFe_2O_4$	16d	273	50	8.44
Inverse	$ZnFe_2O_4$	8a	251	0	8.44
	$Li_{0.4}ZnFe_2O_4$	8a	265	14	8.44
	$LiZnFe_2O_4$	16d	257	34	7.80
	$LiZnFe_2O_4$	16c	251	35	7.70
	$LiZnFe_2O_4$	8a	285	34	8.44

TABLE II. Parameters of Fe K-edge multiple scattering calculations via lithium insertion for both normal and inverse spinel and considering the Fe migration.

L-edge simulations. Fe $L_{2,3}$-edge XANES spectra were simulated within the Ligand Field Multiplet (LFM) theory framework by using the CTM4XAS code[29], taking into consideration spin-orbit coupling, crystal field effects and reduction of the Slater integrals (F(dd), F(pd), and G(pd)) to include the inter-atomic configuration interaction[30]. Full spin-orbit interactions were considered for both Fe^{2+} and Fe^{3+} cations. The $d-d$ and $p-d$ Slater integrals were assumed to be 0.8 of the Hartree–Fock values. Octahedral crystal fields of 1.45 and 1 eV were used for Fe^{2+} and Fe^{3+} cations, respectively. The core-hole lifetime broadening was introduced into the calculation by a Lorentzian with a half-width HWHM of 0.3 (0.5) eV for L_3 (L_2). The instrumental broadening on the other hand was introduced by a Gaussian with a half-width of 0.25 eV. The Zn L-edge calculations (see table III) were carried using the CONTINUUM code (driven by MXAN), considering that Zn in the ZFO spinel structure has a fully occupied $3d^{10}$ band (both for the normal and inverse spinel structure) and XANES can be reliably modeled within the multiple scattering theory.

Structure	Position	No. atoms	No. Li	Cluster Size (Å)
$ZnFe_2O_4$	8a	251	0	8.44
$ZnFe_2O_4$	16c	221	0	8.53

TABLE III. Parameters of Zn L-edge multiple scattering calculations with and without Zn cation migration to 16c sites.

IV. RESULTS AND DISCUSSIONS

A. Carbon-coated $ZnFe_2O_4$ pristine nanocrystals

Normalized Fe and Zn K-edge XANES spectra of the pristine ZFO-C samples are shown in Fig. 1. The experimental Fe and Zn K-edge spectra are compared with calculated XAS cross sections for the normal spinel at the Fe and Zn edges (red lines). Details of the full multiple-scattering calculations are reported in the preceding section. The experimental absorption spectra were normalized using a first order polynomial the pre-edge region and a cubic polynomial the spectrum after the edge. In case of the theoretical calculations, prior to the edge the cross section values are considered zero and normalized up to calculated range with a first order polynomial for both pre-edge and post-edge regions considering the absence of the secondary background in the simulations. The Fe K-edge spectrum contains five clear features (indicated as A-E), with the pre-edge component A at 7115 eV and four major post-edge components around 7128, 7133, 7139.5 and 7145 eV respectively (See figure 1a). The small pre-edge peak A can be either due to the 1s to 3d transition or to 1s to 4p transitions[31]. Both direct 1s to 3d quadrupole transitions and dipole transitions to 4p hybridized with the 3d band are possible, though the intensity of the quadrupole transition is generally very low[32]. The Zn K-edge also contains five major components (A-E) at 9665.2, 9669.5, 9674, 9687.5 and 9696 eV, respectively (figure 1b). The results of the XANES simulations obtained using the normal spinel structure (no inversion) show that

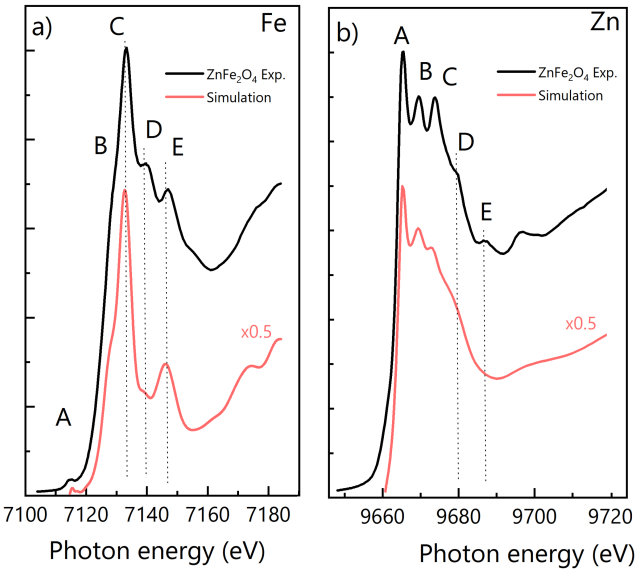

Fig. 1. Fe (a) and Zn (b) K-edge normalized XANES spectra of the pristine ZFO-C samples, compared with the results of the multiple-scattering simulations based on the normal spinel state (red lines). The main features of the experimental spectra are labelled A-E. All of the spectra are normalized to 1 at 7180 eV (Fe) and 9720 (Zn). The intensity of the simulated XANES cross-section is reduced (x 0.5) for better visibility.

a qualitative agreement with the experiments can be observed in the position of several features, however, exhibiting several differences that deserve careful consideration. Disagreements can be expected in intensity and position of the features near the edges, due to the limitations of the calculations (A,B,C). This is due to the fact that reasonable atomic potentials for scattering by using complex potential must be taken beyond the energy of the first plasmon pole approximation that means few electron volt from the edge. Below this limit, close to zero and below the edge, normalization of states is undetermined by the theory. However, the appearance of different features well above the edges, in a safer region for XANES simulations, suggest that those disagreements may have a structural origin.

In particular, we have considered the possibility of an inversion of the normal spinel lattice structure. Therefore, further XANES simulations were carried out gradually migrating the cations to the inverted positions in which the Fe^{3+} ions in 16*d* site are displaced to 8*a* and vice-versa for Zn^{2+} from 8*a* to 16*d* (see figure 2). Spectral simulations of Fe and Zn for different degrees of spinel inversion were obtained by weighted sum of two calculations for normal and inverted spinel. As shown in Fig. 2, the contribution of inverse spinel Fe K-edge XANES includes the D feature (not reproduced for normal spinel) and seems to improve the agreement with experimental data for the other features. For Zn K-edge, the E feature is reproduced only when introducing spinel inversion.

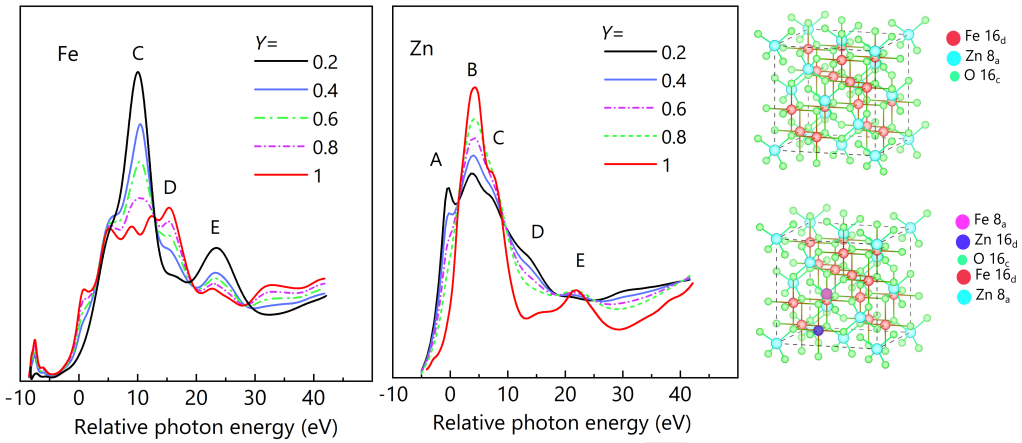

Fig. 2. Spectral simulations of Fe and Zn for different degrees of spinel inversion obtained by weighted sum of normal and inverted spinel as $[Zn^{2+}_{1-y}Fe^{3+}_{y}]_{tet}[Zn^{2+}_{y}Fe^{3+}_{2-y}]_{oct}O_4$ versus y.

Considering the general formula of disordered $ZnFe_2O_4$ as $[Zn^{2+}_{1-y}Fe^{3+}_{y}]_{tet}[Zn^{2+}_{y}Fe^{3+}_{2-y}]_{oct}O_4$ with y being the inversion coefficient corresponding to the degree of cation disorder, we performed a least square fitting procedure separately for both Zn and Fe K-edge normalized XAS spectra optimizing the y parameter. For Zn K-edge the model XAS spectra were calculated using the following expression $\alpha(E) = (1-y)\alpha_{tet} + y\alpha_{oct}$, while for the Fe K-edge we accounted for the different stoichiometry: $\alpha(E) = y\alpha_{tet} + (2-y)\alpha_{oct}$. The results of the fitting procedures are shown in figure 3 and are in satisfactory agreement with the main features of the experimental XAS spectra. The fitting procedure was carried out using a parabolic weighting factor in order to reproduce more closely the experiment at higher energy, taking into account the intrinsic limits of the theory and avoiding possible convolution problems near the edge. The inversion coefficient y was found to be $y = 0.23 \pm 0.05$ for Fe and $y = 0.16 \pm 0.05$ for Zn corresponding roughly to an inversion of about 20%, taking into account the estimated accuracy of the procedure. The calculated inversion degrees are in substantial agreement with previously reported values for the nano-crystalline $ZnFe_2O_4$ particles[20,33] while in other cases larger values were indicated for particles of much smaller size and subjected to further treatments[15,34–36].

B. Structural evolution upon lithium insertion: experimental evidence

The lithium insertion voltage profile is reported in figure 4a. Based on the X-ray diffraction measurments reported in the supporting information, several Li uptake mechanisms are proposed: intercalation (Eqn. 1); Zn-Fe oxide formation (Eqn. 2); Zn-Fe oxide conversion to metal (Eqn. 3); Li-Zn alloying (Eqn. 4).[10,37]

$$ZnFe_2O_4 + 1.45Li^+ + 1.45e^- \rightarrow Li_{1.45}ZnFe_2O_4 \quad (1)$$

$$Li_{1.45}ZnFe_2O_4 + 0.55Li^+ + 0.55e^- \rightarrow Li_2O + Zn_xFe_yO \quad (2)$$

$$n_xFe_yO + 6Li^+ + 6e^- \rightarrow Zn + 2Fe + 3Li_2O \quad (3)$$

$$Zn + Li^+ + e^- \rightarrow LiZn \quad (4)$$

The potential values at which the four samples for ex-situ measurements have been taken are marked in the graph, and are representative of the main reaction domains. Initially, the potential undergoes a rapid decrease down to a voltage of about 1.5 V which precedes a smoother voltage decrease down to 1.3 V corresponding to Q=49 $mAhg^{-1}$ (see Fig. 4a). The lithium uptake ($Li_xZnFe_2O_4$) takes place at this stage in which the lithium atoms start occupying

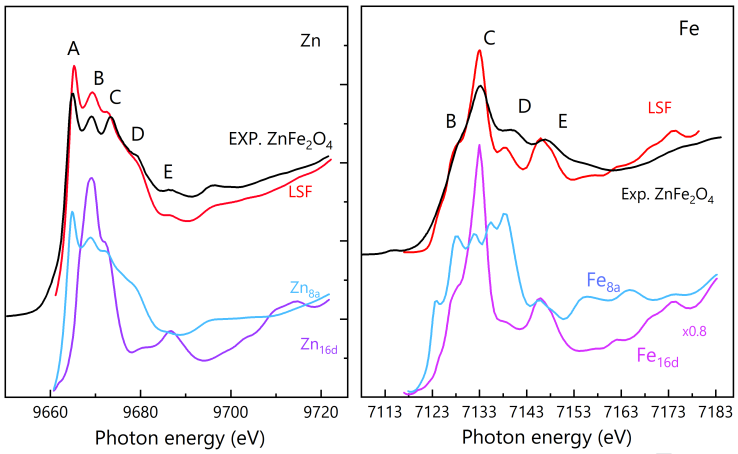

Fig. 3. Upper curves: experimental Fe (left) and Zn (right) K-edge normalized XANES spectra compared with the calculation resulting from a least square fitting procedure (LSF) based on the linear combination of simulations of normal and inverse spinel structures. Lower curves: results of the multiple-scattering simulations for Fe and Zn in normal (16d, 8a) and inverse (8a,16d) spinel positions. Normalized XANES calculations are shown displaced by a constant offset (the Fe_{16d} multiplied by 0.8 for better visibility).

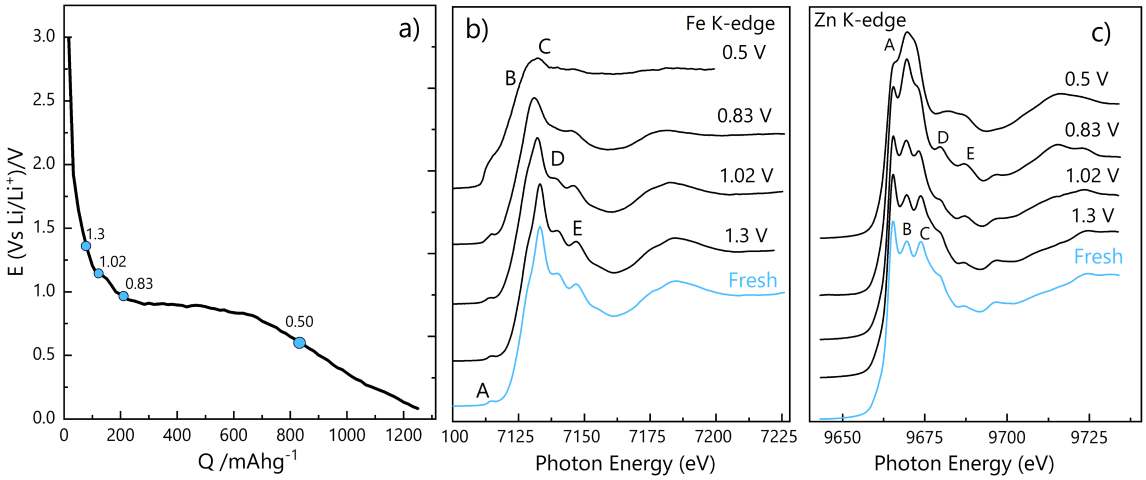

Fig. 4. a) Open circuit potential (E) vs specific capacity (Q) of the ZFO-C electrodes obtained during first Li uptake. Potential and capacity values of the investigated ZFO-C electrodes corresponding to E = 1.3 V and Q= 49 $mAhg^{-1}$, E = 1.02 V, Q= 83 $mAhg^{-1}$, E =0.83 V, Q = 167 $mAhg^{-1}$ and E=0.5 V, Q=836 $mAhg^{-1}$. Panels b) and c) contain the normalized experimental Fe, Zn K-edge XANES spectra of the ZFO-C electrodes for different lithiation stages as indicated in panel a). XANES spectra of the fresh (non-lithiated) electrode is shown for reference. All of the spectra are normalized to one and shifted with a constant offset for better visibility.

the empty 16*c* sites up to a concentration $x = 0.4$, corresponding to $Li_{0.4}ZnFe_2O_4$ in Eq. (1), while the Zn atoms remain in their original 8*a* sites due to their strong preference for the tetrahedral sites[38].

The second regime takes place from 1.3 V to 1.02 V and corresponds to a capacity Q= 83 $mAhg^{-1}$ and the additional lithium uptake reaches an average Li content of $x = 0.9$ resulting in $Li_{0.9}ZnFe_2O_4$ (Eq. 2). The further lithium uptake in this regime can result in an expansion of the spinel structure and the presence of additional Li^+ ions can lead to a strong repulsive interaction with the Zn ions occupying nearby sites. Zn atoms can thus migrate to 16*c* sites, similar to the case of Fe_2O_3 lithiation and observed in the lithiation of the spinel $ZnFe_2O_4$[7,11,39].

The third lithiation regime can be identified in Fig. 4a by a smooth voltage decrease about 1.02 V to ~ 0.83 V, preceding a wide voltage plateau. Based on our measurements, a specific capacity of ~167 $mAhg^{-1}$ is obtained at 1.02 V, which corresponds to the formation of an average compodition $Li_{1.45}ZnFe_2O_4$ (Eq.1). From 0.83 V, the oxide formation and oxide conversion processes, as summarized in Eqn. (2) and (3), take place at almost constant voltage, together with SEI formation on top of the active material[40,41]. Finally, the sloping line, which includes the E = 0.5

V point where the fourth ex-situ sample has been collected, is representative of the initial stages of the Li-Zn alloying process.

XANES measurements were carried out on ZFO-C electrodes close to specific lithium charging levels, in order to study the structural evolution of the spinel structure via lithium insertion. Despite the transfer of the samples within a controlled atmosphere, it should be mentioned that possible internal rearrangements of the sample may occur, especially related to a phase equilibration between bulk and surface. Nevertheless, since the Li uptake level has been previously controlled by galvanostatic discharge, this rearrangement only leads to possible surface/bulk equilibration, without affecting the average Li content. Furthermore, based on several simulations with distinct Li concentrations, the small electron transfers to the SEI layer during the first cycle does not affect the effective average Li content. Fe and Zn K-edge XANES spectra are shown in Fig. 4b,c and compared with the XANES of the non-lithiated (fresh) electrodes. The evolution of the Fe K-edge XANES in Fig. 4b is quite simple with the characteristic XANES of an oxide (spinel) converting gradually into a metallic phase. In , the pre-peak A is shifted and eventually merged with the continuum region at 0.5 V. The B feature is also broadened and practically disappears at 0.83 V. Peak C (white line) is shifted to lower energies and broadens especially in the metallic phase (0.5 V). Peak D disappears at 0.83 V, while peak E is finally washed out at 0.5 V.

Similar to Fe K-edge, the Zn K-edge XANES spectra (see Fig. 4c) show no significant modifications within the initial lithiation stage (1.3 V). Further lithiation to 1.02 V, on the other hand, results in a reduction of the intensity of the C feature. More drastic changes in the intensity of features B, C, D are observed as a result of the accelerated lithium uptake up to 0.83 V. Finally, for increased lithiation at 0.5 eV, all of the A-E features are broadened indicating that a structural transition has taken place.

C. Structural evolution upon lithium insertion: XANES simulations

In this section we show the results of Fe and Zn K-edge XANES simulations with the aim of understanding the local structural rearrangements taking place in ZFO-C electrodes upon lithiation.

In Fig. 5a we report the results of the Zn K-edge XANES simulations for increasing levels of occupation (Zn) of octahedral (16*c*) sites. A modulation in intensity and position of the various features of the XANES spectra is clearly associated with the migration of Zn atoms from tetrahedral to octahedral sites expected in normal spinel $ZnFe_2O_4$[11,39].

Looking at the experimental results, shown in Fig. 5b-d for increasing Li content, we can appreciate the similarity of the observed XANES features with those obtained in the simulations. The XANES spectrum collected for modest charging levels (1.3 V) is quite similar to that of the pristine (fresh) electrode so migration of Zn atoms to these octahedral sites is not activated (while an inversion of about 20% is already present in the pristine nanomaterial). This result is in agreement with previous suggestions indicating that Zn migration can occur for values higher than 0.4 lithium unit[7,10]. For higher lithiation levels, the Zn K-edge XANES spectra undergo drastic modifications.

The experimental XANES spectrum reported in Fig. 5c (0.83 V) shows a pronounced B feature which may be considered as a fingerprint for the migration of several Zn atoms from tetrahedral 8*a* to octahedral sites specially 16*c*. In Fig. 5c we include the results of three simulations with Zn atoms in 8*a*, 16*c* and 16*d* (see previous section III) positions. The XANES spectrum still contains components of non-migrated 8*a* Zn ions, however the complexity of the mixed normal-inverse ($8a, 16d$) spinel structure in which a portion of the Zn atoms are migrated to 16*c* sites does not allow for a quantitative determination of the concentration of migrated atoms. However, the growth of the B feature can be safely assigned to the octahedral sites.

The Zn K-edge XANES reported in Fig. 5d is the result of the further development of lithium insertion (fourth regime, V= 0.5 V). Here, the presence of Zn in tetrahedral sites may be considered negligible, while the broadening of the C, D, E features indicates that significant disorder is taking place along with the possible expected contribution of metallic zinc (reported as Zn^0 in Fig. 5d) is present. Most of the features associated with octahedral sites, although broadened, are retained at this stage.

Similar multiple-scattering simulations were carried out at Fe K-edge for different level of the lithium uptake (see Fig. 6a), considering the Zn migration to the 16*c* sites for increasing lithiation levels. XANES simulations for selected Li concentrations were carried out considering as a reference either half or all the Zn atoms are moved to the 16*c* octahedral positions, with the Fe ion sites unchanged. The changes observed in the XANES simulations (Fig. 6a) confirm the sensitivity of the technique to the evolution of the local structure.

The Fe K-edge XANES of the ZFO-C lithiated sample at the initial stage (1.3 V) show modest changes with respect to the non-lithiated ones. A first important change is obtained during the second lithiation regime (0.83 V). The experimental Fe K-edge XANES spectrum (0.83 V) reported in Fig. 6b show features that may be assigned to several different components including the mentioned inversion between Fe and Zn ions and the migration of Zn and Fe ions to 16*c* sites. XANES simulations related to these structure contributions are also shown in Fig. 6b. In particular,

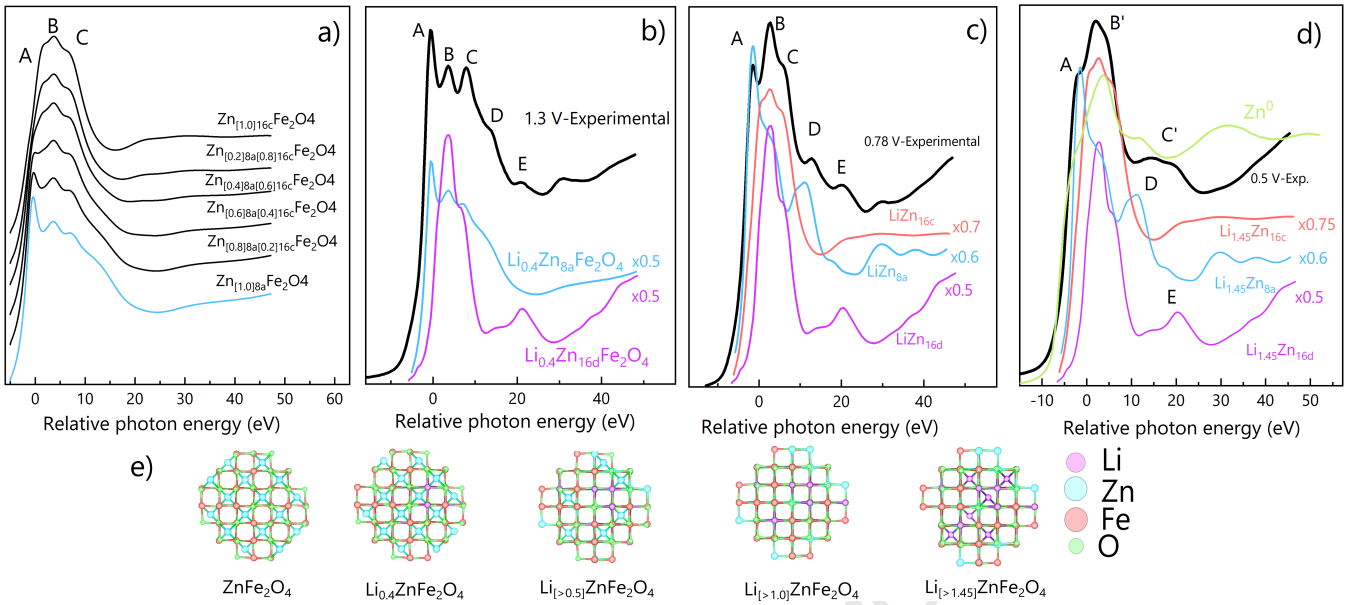

Fig. 5. a)XANES Zn K-edge multiple-scattering simulations as a function of the Zn atoms displacement from tetrahedral 8*a* to octahedral 16*c* sites (from bottom to top). b) Experimental K-edge XANES spectrum of ZFO-C lithiated (1.3 V) compared with corresponding simulations carried out placing Zn atoms at 8*a* sites of the normal spinel (blue) and 16*d* sites of the inverse spinel (violet). c) Experimental K-edge XANES spectrum of ZFO-C lithiated (0.83 V) compared with corresponding simulations carried out placing Zn atoms at: 8*a* sites of the normal spinel (blue), 16*d* sites of the inverse spinel (violet), 16*c* (migrated) sites of the normal spinel (red). d) Experimental K-edge XANES spectrum of ZFO-C lithiated (0.5 V) compared with corresponding simulations carried out placing Zn atoms at: 8*a* sites of the normal spinel (blue), 16*d* sites of the inverse spinel (violet), 16*c* (migrated) sites of the normal spinel (red), metal Zn reference foil (Zn^0, green). e) Visualization of the structure of ZFO spinel and its transformation to the rock salt cubic structure via lithium insertion (used in the XANES simulations for different lithiation stages). All XANES spectra are normalized to one, results of the simulations are multiplied by factors indicated in figure for better visibility.

the migration of Fe atoms to the 16*c* octahedral sites in the inverse spinel can explain the broadening of the various post-edge features. This migration may be understood considering that octahedral sites are favored for Fe^{2+} ions[8,9] and that, similar to what happens to tetrahedral Zn ions, strong coulomb repulsive interactions can also favor this rearrangement. This migration is confirmed by broadening of the component (D), present at this stage of lithiation in inverse structure simulation without migration (Fig. 6b-violet) while absent in the simulations considering the Fe/Zn ions migration (Fig. 6b-red/blue).

The Fe K-edge XANES, reported in Fig. 6c, shows major changes as a result of the further development of lithium insertion (fourth regime, V= 0.5 V). While a contribution due to the spinel structure is still visible (see E feature), iron is mostly found in metallic state as confirmed by the red-shift of the edge and appearance of the characteristic shoulder (A) and by a broadening of the post-edge features. The comparison with the XANES spectrum of a metallic Fe foil (green line) indicates that formation of metallic Fe particles takes place at this stage as also expected based on the eq. (4) and Ref.[11]. However, the XANES shape does not comply precisely with those of the Fe foil and lithiated spinel structures. This can be possibly explained observing that metal Fe is obtained in form of small nanoparticles possibly containing Zn, in which further broadening is expected. Moreover, we should also account for contributions of the inverse spinel structure which may accommodate a large portion of the inserted lithium, in agreement with previous calculations indicating a three times higher lithium capacity of the mixed spinel structure with respect to that of normal spinel[8,9].

D. L-edge XANES: experiments and simulations

The structural rearrangements are expected to begin at the surface of the active materials, therefore we also carried out surface-sensitive L-edge XAS studies of the mentioned ZFO-C electrodes. Fe and Zn L-edge total electron yield (TEY) measurements were performed, with typical probing depths of 6 and 9 nm respectively[23]. Being the average size of the ZFO-C nanoparticles around 50 nm[23], only photabsorbing atoms in the superficial layers contribute to the

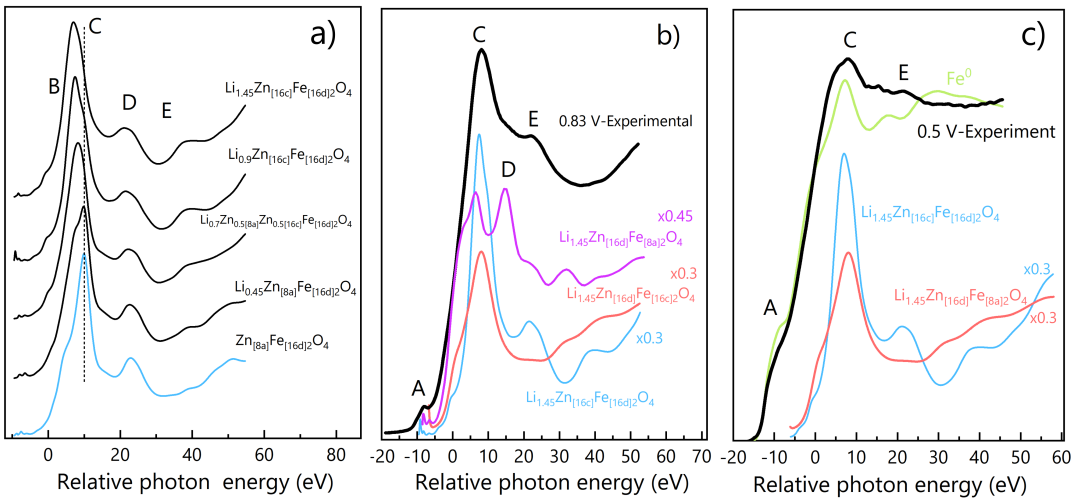

Fig. 6. a)XANES Fe K-edge multiple-scattering simulations as a function of the Li concentration and Zn atoms displacement from tetrahedral 8*a* to octahedral 16*c* sites (from bottom to top). b) Experimental K-edge XANES spectrum of ZFO-C lithiated (0.83 V) compared with corresponding simulations with: Fe atoms at 16*d* sites of the normal spinel (blue) and 8*a* sites of the inverse spinel (violet) and migrated Fe atoms to 16*c* of the inverse spinel (red). c) Experimental K-edge XANES spectrum of ZFO-C lithiated (0.5 V) compared with corresponding simulations with: Fe atoms at 16*d* sites of the normal spinel (blue) and migrated Fe atoms to 16*c* of the inverse spinel (red). The XANES of metal Fe is shown as a reference for a fully reduced iron (Fe^0,green). All XANES spectra are normalized to one, results of the simulations are multiplied by factors indicated in figure for better visibility.

experimental XAS signal (the probed surface atoms are ∼7 % and ∼ 10 % of the bulk, for Fe L-edge and Zn L-edge respectively).

Experimental Fe and Zn L-edge XANES spectra are compared with the results of the simulations in Fig. 7. XAS measurements could only be carried out up to 1.02 V, because for increasing lithiation levels the TEY signals can not be detected. This effect is related to the progressive development of the solid electrolyte interphase (SEI) that gradually covers the ZFO-C nanoparticles (see[23,41,42]) and hence diminishes the intensity of the XAS signal. Furthermore, the participation of the active material (ZFO) into the SEI layer can reasonably be considered negligible[41].

The Fe $L_{2,3}$ XAS spectra of the pristine sample clearly show the dominance of iron in the Fe^{3+} form (Figure 7a) with two major components at 708.6 and 710.2 (labelled A and B respectively) and two minor components at 721.8 and 723.6 eV. The initial lithiation stages up to 1.3 V results in a reduction of the Fe^{3+} component although the dominant contribution remains that of Fe^{3+} . However, at the second lithiation stage (1.02 V) the XAS spectra shows signatures of the oxidation state in line with that of Fe^{2+}. The intensity ratio between the A and B peaks is clearly inverted. The broadening visible at L2 edges are due to an additional component at around 717 eV from the strong absorption of F k-edge , expected from the side reaction with the electrolyte (e.g., LiF, LiP_xF_{5-x}). These results indicate that the reduction of the Fe components starts at the early stages of lithiation, as early as 1.3 V. Furthermore, the extension of the Fe reduction is much higher near the surface, being Fe^{2+} the dominant phase at 1.02 V. In contrast to the Fe K-edge results, this suggests that the migration of Fe atoms from 8*a* positions to 16*c* atoms, in superficial layers, can occur even within the initial stages of lithiation since the reduction of Fe atoms via the simultaneous electron uptake causes the reduction of Fe^{3+} to Fe^{2+} for which the preferential site is the octahedral 16*c*[8,9]. By comparison with hard x-ray Fe K-edge data, the reduction propagates into the bulk structure at later stages. Finally, Zn L-edge multiple-scattering simulations have been performed and compared with XANES experimental data. Separate calculations were carried out considering first the normal spinel structure with Zn atoms at 8*a* sites and then a second structure with the photoabsorbing atom migrated to a 16*c* site. The results are shown in figure 7 and compared with the experimental spectra. As can be seen in the figure, the Zn L_{23} edge of the pristine sample presents four major contributions at 1015.7, 1019.5, 1024.6 and 1030 eV and a broader intense feature at 1040.6 eV (labeled A,B,C, D and F respectively). The position of those features is in reasonable agreement with a majority of Zn atoms in the 8*a* sites in the simulations. Within the initial stages of the lithiation, up to 1.3 V, the modification of the intensity in the spectral shape can be interpreted as a signature of migration of Zn atoms from 8*a* to 16*c* octahedral sites (decrease of B, F peaks, relative increase of the other features). Upon further lithiation, this trend is confirmed and there is a dominant contribution of Zn atoms in octahedral 16*c* sites. Similarly to the results obtained considering the Fe L-edge, the migration of the Zn atoms is found to occur even at the initial lithiation stages. From the combined

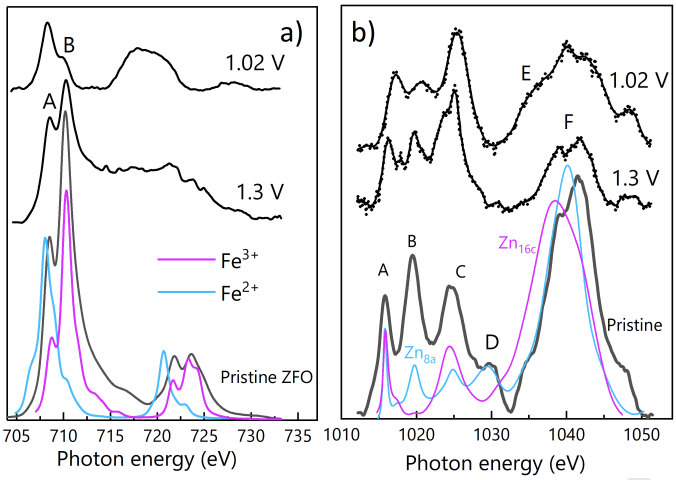

Fig. 7. a) Experimental Fe L-edge spectra of pristine and lithiated ZFO-C at 1.3 V and 1.02 V compared with Fe^{2+} (blue) and Fe^{3+} (violet) LFM simulations . b) Experimental Zn L-edge spectra of the pristine and lithiated ZFO-C at 1.3 V and 1.02 V compared with the result of multiple-scattering simulations of the spinel structure (blue) and with Zn atoms moved to 16*c* (violet).

observation of the results obtained at the K and L-edges, it can be inferred that the Li insertion proceeds gradually from the surface to the bulk of the ZFO-C particles, and that for a given charge level the Li density is not uniform inside the active particles being larger at the surface.

V. CONCLUSIONS

In this work, we have studied the evolution of the local structure upon lithiation in Li-ion anodes fabricated using carbon coated $ZnFe_2O_4$ nanoparticles, by K-edge and L-edge x-ray absorption near edge spectroscopy (XANES). Simulations of the XANES data were performed using full multiple scattering (Fe, Zn K-edge, Zn L-edge) and ligand field multiplet (LFM) calculations (Fe L-edge). Simulations were compared with experimental spectra obtained on ZFO-C nanoparticles previously characterized by electrochemical measurements. We have shown that a satisfactory agreement for the XANES Fe and Zn K-edges of pristine ZFO-C bulk nanoparticles can be obtained introducing a mixed spinel structure $[Zn^{2+}_{1-y}Fe^{3+}_{y}]_{tet}[Zn^{2+}_{y}Fe^{3+}_{2-y}]_{oct}O_4$ (y=0 for non-inverted spinel) with Fe and Zn partially occupying tetrahedral and octahedral sites. A least square fitting procedure applied to the Fe and Zn XANES spectra resulted in an inversion coefficient $y = 0.23 \pm 0.05$ for Fe and $y = 0.16 \pm 0.05$ for Zn corresponding roughly to an inversion of about 20%. The evolution of the XANES spectra upon lithiation was interpreted introducing displacements of the cations as an effect of occupation of Li into empty lattice sites. The lithium insertion into the mixed spinel structure was investigated at specific stages of the lithium uptake and capacity. We have shown that at the initial stages of lithium bulk uptake ($Li_{0.4}ZnFe_2O_4$), Li ions occupy vacant octahedral (16*c*) sites while the normal and inverse spinel structures are preserved. Migration of metal ions from tetrahedral to octahedral sites (16*c*) was observed to start at higher lithiation levels, when Li can also occupy vacant tetrahedral sites. Migration of Zn ions is mainly due to the large repulsive interaction while for Fe ions also a reduction mechanism Fe^{3+} to Fe^{2+} is observed. Spinel inversion is found to play a role in the increased lithium uptake capacity of the metal alloy oxides with spinel structures. For lithiation levels higher than $Li_{1.45}ZnFe_2O_4$ we observe the signature of metalization for both Zn and Fe. It is also important to remark that the present study of L-edge XANES spectra has shown that the relocation and valence change of metal ions occur at early lithiation stages at the surface of the active material, gradually extending to the bulk for larger Li uptakes. These results deepens the fundamental understanding of the functionality and structural dynamics of the metal alloy oxides nanomaterials with mixed spinel structures that can lead to improvement in anode performances.

VI. ACKNOWLEDGMENT

The support of the European Commission under the Project Stable Interfaces for Rechargeable Batteries" (SIRBATT) (FP7-ENERGY-2013, grant agreement No. 608502) is gratefully acknowledged. We acknowledge the Elettra and ESRF Synchrotron Radiation Facility for provision of beam time and we would like to thank A. Giglia and A. Puri for thier assistance at LISA and BEAR beamlines.

[1] J. M. Tarascon and M. Armand, Nature **414**, 359–67 (2001).
[2] M.Dollea, J.Hollingsworth, T.J.Richardson, and M.M.Doef, .
[3] B. H. Zhang, Y. Liu, Z. Chang, Y. Q. Yang, Z. B. Wen, and Y. P. Wu, Electrochimica Acta **130**, 693 (2014).
[4] N. Yabuuchi, M. Yano, S. Kuze, and S. Komaba, Electrochimica Acta **82**, 296–301. (2012).
[5] M. G. Thomas, P. G. Bruce, and J. B. Goodenough, Solid State Ionics **17**, 13 (1985).
[6] R. Chen, M. Knapp, M. Yavuz, R. Heinzmann, D. Wang, S. Ren, V. Trouillet, S. Lebedkin, S. Doyle, H. Hahn, H. Ehrenberg, and S. Indris, Journal of Physical Chemistry C **118**, 12608 (2014).
[7] M. M. Thackeray, W. I. F. David, and J. B. Goodenough, Materials Research Bulletin **17**, 785 (1982).
[8] C. J. Chen, M. Greenblatt, and J. V. Waszczak, Solid State Ionics **18-19**, 838 (1986).
[9] C. J. Chen, M. Greenblatt, and J. V. Waszczak, Materials Research Bulletin **21**, 609 (1986).
[10] D. Bresser, E. Paillard, R. Kloepsch, S. Krueger, M. Fiedler, R. Schmitz, D. Baither, M. Winter, and S. Passerini, Advanced Energy Materials **3**, 513 (2013).
[11] Y. Zhang, C. J. Pelliccione, A. B. Brady, H. Guo, P. F. Smith, P. Liu, A. C. Marschilok, K. J. Takeuchi, and E. S. Takeuchi, Chem. Mater. **29**, 4282 (2017).
[12] M. J. Akhtar, M. Nadeem, S. Javaid, and M. Atif, Journal of physics. Condensed matter : an Institute of Physics journal **21** (2009), 10.1088/0953-8984/21/40/405303.
[13] S. Nakashima, K. Fujita, K. Tanaka, K. Hirao, T. Yamamoto, and I. Tanaka, Physical Review B - Condensed Matter and Materials Physics **75** (2007), 10.1103/PhysRevB.75.174443.
[14] J. Philip, G. Gnanaprakash, G. Panneerselvam, M. P. Antony, T. Jayakumar, and B. Raj, Journal of Applied Physics **102** (2007), 10.1063/1.2777168.
[15] H. H. Hamdeh, J. C. Ho, S. A. Oliver, R. J. Willey, G. Oliveri, and G. Busca, Journal of Applied Physics **81**, 1851 (1997).
[16] F. Li, L. Wang, J. Wang, Q. Zhou, X. Zhou, H. Kunkel, and G. Williams, Journal of Magnetism and Magnetic Materials **268**, 332 (2004).
[17] J. H. Shim, S. Lee, J. H. Park, S.-J. Han, Y. H. Jeong, and Y. W. Cho, Physical Review B **73**, 064404 (2006).
[18] M. Hofmann, S. J. Campbell, H. Ehrhardt, and R. Feyerherm, Journal of Materials Science **39**, 5057 (2004).
[19] M. K. Roy, B. Haldar, and H. C. Verma, Nanotechnology **17**, 232 (2006).
[20] S. A. Oliver, V. G. Harris, H. H. Hamdeh, and J. C. Ho, Applied Physics Letters **76**, 2761 (2000).
[21] B. Jeyadevan, K. Tohji, and K. Nakatsuka, Journal of Applied Physics **76**, 6325 (1994).
[22] A. Witkowska, A. Di Cicco, and E. Principi, Phys. Rev. B **76**, 104110 (2007).
[23] A. Di Cicco, A. Giglia, R. Gunnella, S. L. Koch, F. Mueller, F. Nobili, M. Pasqualini, S. Passerini, R. Tossici, and A. Witkowska, Advanced Energy Materials **6** (2015), 10.1002/aenm.201500642.
[24] F. d'Acapito, A. Trapananti, S. Torrengo, and S. Mobilio, Notiziario Neutroni e Luce di Sincrotrone **19**, 14–23 (2014).
[25] S. Nannarone, in *AIP Conference Proceedings*, Vol. 705 (AIP, 2004) pp. 450–453.
[26] M. Benfatto, S. Della Longa, and C. R. Natoli, Journal of Synchrotron Radiation **10**, 51 (2003).
[27] C. R. Natoli, D. K. Misemer, S. Doniach, and F. W. Kutzler, Phys. Rev. A **22**, 1104 (1980).
[28] S. J. Stewart, S. J. A. Figueroa, J. M. Ramallo López, S. G. Marchetti, J. F. Bengoa, R. J. Prado, and F. G. Requejo, Physical Review B **75**, 073408 (2007), arXiv:0611532 [cond-mat].
[29] E. Stavitski and F. M. de Groot, Micron **41**, 687 (2010).
[30] R. Cowan, *Los Alamos Series in Basic and Applied Sciences, Berkeley: University of California Press* (1981).
[31] F. de Groot, Chemical Reviews **101**, 1779 (2001).
[32] T. E. Westre, P. Kennepohl, J. G. DeWitt, B. Hedman, K. O. Hodgson, and E. I. Solomon, Journal of the American Chemical Society **119**, 6297 (1997).
[33] D. Carta, M. F. Casula, A. Falqui, D. Loche, G. Mountjoy, C. Sangregorio, and A. Corrias, The Journal of Physical Chemistry C **113**, 8606 (2009), arXiv:1011.1669.
[34] J. Wu, N. Li, J. Xu, Y. Jiang, Z.-G. Ye, Z. Xie, and L. Zheng, Applied Physics Letters **99**, 202505 (2011).
[35] Z. Ž. Lazarević, Č. Jovalekić, V. N. Ivanovski, A. Rečnik, A. Milutinović, B. Cekić, and N. Ž. Romčević, Journal of Physics and Chemistry of Solids **75**, 869 (2014).
[36] S. Zhou, K. Potzger, D. Bürger, K. Kuepper, M. Helm, J. Fassbender, and H. Schmidt, Nuclear Instruments and Methods in Physics Research Section B: Beam Interactions with Materials and Atoms **267**, 1620 (2009).
[37] "Supporting information,".
[38] V. S. Urusov, Physics and Chemistry of Minerals **9**, 1 (1983).
[39] L. Wang, A. McCarthy, K. J. Takeuchi, E. S. Takeuchi, and A. C. Marschilok, MRS Advances **3**, 773–778 (2018).

[40] S. J. Rezvani, M. Ciambezi, R. Gunnella, M. Minicucci, M. A. Muñoz, F. Nobili, M. Pasqualini, S. Passerini, C. Schreiner, A. Trapananti, A. Witkowska, and A. Di Cicco, The Journal of Physical Chemistry C **120**, 4287 (2016).
[41] S. J. Rezvani, F. Nobili, R. Gunnella, M. Ali, R. Tossici, S. Passerini, and A. Di Cicco, The Journal of Physical Chemistry C **121**, 26379 (2017).
[42] S. J. Rezvani, R. Gunnella, A. Witkowska, F. Mueller, M. Pasqualini, F. Nobili, S. Passerini, and A. D. Cicco, ACS Applied Materials and Interfaces **9**, 4570 (2017).

- Comparison of experimental X-ray absorption spectra of Zn and Fe edges with simulations shows presence of mixed spinel structure in ZnFe2O4 nanoparticles.
- The XANES spectra upon lithiation is interpreted introducing displacements of the cations as an effect of occupation of Li into empty lattice sites.
- Migration of Zn ions upon lithiation is mainly due to the large repulsive interaction while for Fe ions also a reduction mechanism Fe^{3+} to Fe^{2+} is observed.
- Spinel inversion plays an important role in the increased lithium uptake capacity of the metal alloy oxides with spinel structures.
- The relocation and valence change of metal ions occur at earlier lithiation stages at the surface of the active material and gradually extend to the bulk.